Generalized time-frequency coherency for assessing neural interactions in electrophysiological recordings

Saeid Mehrkanoon[a,b,*], Michael Breakspear[a,b,d,e], Andreas Daffertshofer[c], Tjeerd W. Boonstra[a,b,c]

[a] *School of Psychiatry, University of New South Wales, Sydney, Australia*
[b] *The Black Dog Institute, Sydney, Australia*
[c] *Research Institute MOVE, VU University Amsterdam, The Netherlands*
[d] *Queensland Institute of Medical Research, Brisbane, Australia*
[e] *Royal Brisbane and Women's Hospital, Brisbane, Australia*

Abstract

Time-frequency coherence has been widely used to quantify statistical dependencies in bivariate data and has proven to be vital for the study of neural interactions in electrophysiological recordings. Conventional methods establish time-frequency coherence by smoothing the cross and power spectra using identical smoothing procedures. Smoothing entails a trade-off between time-frequency resolution and statistical consistency and is critical for detecting instantaneous coherence in single-trial data. Here, we propose a generalized method to estimate time-frequency coherency by using different smoothing procedures for the cross spectra versus power spectra. This novel method has an improved trade-off between time resolution and statistical consistency compared to conventional methods, as verified by two simulated data sets. The methods are then applied to single-trial surface encephalography recorded from human subjects for comparative purposes. Our approach extracted robust alpha- and gamma-band synchronization over the visual cortex that was not detected by conventional methods, demonstrating the

*Corresponding author at: School of Psychiatry, The University of New South Wales, Black Dog Institute Building, Hospital Rd, Randwick, NSW 2031, Australia, Tel: +61 2 9382 9260, Email: s.mehrkanoon@unsw.edu.au

efficacy of this method.
Keywords: coherence, electroencephalography, time-frequency analysis, neuronal synchronization

1. Introduction

Coherence analysis has been widely used for investigating functional connectivity between neurophysiological signals to understand perception, action and cognition[24,30,9]. Correlations occurring at different frequencies between two or more neuronal signals are assumed to indicate oscillatory coupling of neuronal groups. Since neural synchronization is not constant but varies over time, time-resolved estimate of coherence is used to capture the dynamics of neuronal synchronization. However, some form of smoothing is required to estimate time-frequency coherence. This smoothing entails a trade-off between time-frequency resolution and statistical consistency[21]. A number of variations have been proposed to improve this trade-off and obtain a more efficient estimation of time-frequency coherence[11,7,2].

Here, we propose a generalization of the coherency function to further improve the estimation of time-frequency coherency (TFCOH). The classic coherency function is a well-established approach to measure linear correlation between two arbitrary signals as a function of frequency[27]. Coherency is a complex-valued measure of the linear correlation between two stationary signals[6], and the so-called magnitude-squared coherence is the square of coherency's magnitude. Coherency is defined as the ensemble averaged cross spectra normalized by the square root of the product of ensemble averaged power spectra. As such, it does not capture TFCOH and/or temporal variations in correlation. To obtain time-resolved coherence, many studies have used a trial averaging method in event-related

experimental designs[25]. In event-related coherency, the cross and power spectra are the average over epochs or trials, which eliminates the need to smooth the coefficients over time. However, event-related averaging cannot be used in experimental protocols that do not include any events, such as resting state activity, which requires the estimation of time-frequency coherency in single trials. In single-trial coherency, a time-resolved estimate can be obtained by smoothing in one or both of the time/frequency domains or by averaging across orthogonal data tapers in a multiwavelet approach[7]. Temporal smoothing is the most commonly used in the literature[19,11]. It involves a trade-off between temporal resolution and statistical consistency as a function of the smoothing window size. Alternatively, time-frequency dependency may be estimated by statistical tests of the non-smoothed cross spectra[2]. However, without normalization by the product of the power spectra the method no longer provides an estimate of correlation between 0 and 1, which complicates the comparison of functional connectivity across data sets.

Whereas an identical smoothing operator for the cross and power spectra is used in conventional methods, we propose a generalized coherency function by introducing different smoothing operators for the cross and power spectra. As a special case, we investigate TFCOH obtained by normalizing the non-smoothed cross spectra by the product of ensemble averaged power spectra. Two distinct simulation studies are performed to compare the efficiency of this method against conventional methods; one for a signal pair with time-varying coherency, and the other for a signal pair with frequency-varying coherence buried in white noise of varying strengths. The resulting TFCOH are evaluated using statistical tests, such as sensitivity, specificity, and z-score. Finally, the methods are applied to surface electroencephalography (EEG) of three human subjects to characterize

synchronous alpha activity between occipital channels.

2. Materials and Methods

2.1. ***Spectral decomposition***

Overall, methods for estimating TFCOH vary in two different aspects: (1) spectral decomposition approaches, and (2) temporally smoothing (or integration) approaches. We give a brief review on these two aspects in the following subsections. Coherence can be obtained by different methods of spectral decomposition, such as short-time Fourier transform (STFT) or wavelet transform (WT)[8]. STFT uses the Fourier transform of a windowed signal for spectral estimation. In general, there is a trade-off between spectral and temporal resolution depending on window length. Short windows give poor spectral resolution and good temporal resolution, and vice versa for long window. Temporal and spectral resolutions remain constant across frequencies as a fixed window length is used. In addition, STFT assures stationarity within each data segment. In contrast, wavelet-based spectral decomposition uses scale-dependent window functions optimizing the trade-off for each frequency, independently. Wavelet-based methods decompose a signal to a set of time-domain basis functions with various frequency resolutions. Wavelet transform is computationally similar to STFT. Unlike the sine and cosine functions used in the STFT, however, wavelet transform uses wavelet functions to represent a signal in the time and frequency domains. Often, wavelet based methods use complex Morlet wavelet for spectral decomposition[31,17,14,18,16,5,3], closely related to the Gabor transform. Irrespective of the differences between spectral decompostion methods, it was shown that the Fourier, Hilbert, and wavelet-based techniques are in fact formally (i.e. mathematically) equivalent when using the most frequently employed class of wavelets[8]. The

generalized coherency function proposed in this paper is independent of the spectral decomposition and can thus be obtained using either STFT or the WT.

2.2. ***Smoothing method***

Temporal smoothing is commonly used to estimate the cross and power spectra for the coherency function estimation[19,11]. Welch's (or weighted) overlapped segment averaging (WOSA) is the basis of the smoothing procedure[10]. Using WOSA, a signal is first divided into T equivalent segments. Each segment is then weighted by a window function. The Fourier transform of each weighted segment is computed, and hence the estimation of the power-spectrum is obtained by averaging over T. It was previously shown that statistical dependence between two discrete-time signals $x[p]$ and $y[p]$, $p = 0, 1, ..., L-1$, where L denotes total number of samples, is estimated by the coherency function at frequency f based on the WOSA approach[10,22,27,1]:

$$\hat{\Gamma}_{xy}[f] = \frac{\sum_{n=1}^{T} s_{xy}[n,f]}{\sqrt{\sum_{n=1}^{T} s_x[n,f] \sum_{n=1}^{T} s_y[n,f]}} \tag{1}$$

where cross spectra $s_{xy}[n,f]$ at nth segment and frequency f is expressed by,

$$s_{xy}[n,f] = DFT\left\{x_n[q]\right\}.DFT^*\left\{y_n[q]\right\},\ n = 1,2,...,T,\ q = 1,2,..,M \tag{2}$$

where * denotes the complex conjugation[31], M the number of samples taken place at nth segment, and $DFT\{x_n[q]\}$ stands for the Discrete Fourier Transform of nth segment of signal $x[p]$:

$$DFT\left\{x_n[q]\right\} = \hat{X}_n[f] = \sum_{q=1}^{M} x_n[q]w[q]e^{-j\frac{2\pi}{M}fq},\ f = 1,2,... \tag{3}$$

where $w[q]$ is a weighting/window function (e.g., Hamming window), f the frequency index, and $j = \sqrt{-1}$. Subsequently, the power spectrum in the nth segment is estimated by $|\hat{X}_n[f]|^2$. By construction, Eq.(1) does not address changes of coherency over time because all time segments n are merely averaged. In the literature, it is common to estimate TFCOH using a smoothing procedure. We further discuss this in the following section.

2.3. ***Time-frequency coherency estimators***

Generalized TFCOH may be expressed by:

$$\hat{\Gamma}_{xy}[n,f] = \frac{S^{\star}\left(s_{xy}[n,f]\right)}{\sqrt{S^{\star\star}\left(s_x[n,f]\right) S^{\star\star}\left(s_y[n,f]\right)}},\ n = 1,2,...,T \tag{4}$$

where $S^{\star}(.)$ and $S^{\star\star}(.)$ both denote *smoothing* operators[28,29,16,8]. *Smoothing* indicates some form of averaging in frequency, time[11,23,19,32], or both, using a multiwavelet method through the application of several orthogonal wavelet functions[7]. The smoothing procedure can be implemented by simple or weighted averaging[11,16,28], or alternatively by convolving the spectral coefficients with a window function (e.g., Gaussian window)[7]. Note that, without any smoothing procedure, Eq.(4) gives the phase difference between Fourier spectra of signals $x[p]$ and $y[p]$, and the magnitude of TFCOH expressed by Eq.(4) renders identically one, regardless of the use of wavelet and/or Fourier transforms.

We will first discuss the conventional smoothing procedure and then consider two examples in which the cross-spectra and the auto-spectra are smoothed with different operators. First, we derive three specific instances of the TFCOH function from Eq.(4) as follows:

2.3.1. ***Method 1 (conventional approach)***

Conventional TFCOH is obtained from Eq.(4) when the smoothing operators are identical, such that $S^{\star}(.) = S^{\star\star}(.)$. That is, spectral coefficients are convolved with an integration window at each specific frequency f as follows.

$$\begin{aligned} S^{\star}(s_{xy}[n,f]) &= s_{xy}[n,f] \circledast h^{\star}[l^{\star}] \\ S^{\star\star}(s_{x}[n,f]) &= s_{x}[n,f] \circledast h^{\star\star}[l^{\star\star}] \end{aligned} \tag{5}$$

where $\circledast$ denotes the convolution operator, and the resulting output is restricted to the **same** time duration as the cross/power spectra, (e.g., T), and $h^{\star}[l^{\star}] = h^{\star\star}[l^{\star\star}]$ is a rectangular window of length $l^{\star} = l^{\star\star} = l$

$$h^{\star}[m] \triangleq \begin{cases} 1 & 0 \leqslant m \leqslant l-1 \\ 0 & \text{elsewhere} \end{cases} \tag{6}$$

used as the integration window. We chose $l = 0.75$sec in the present paper. Note that Fourier decomposition was performed using Hamming window of length 0.5sec. To increase the performance of the TFCOH estimator, it is common to vary the length l with respect to frequency. Although, a smoothing procedure is required, it is not easy to analytically track the effects of smoothing. That is, different choices of smoothing procedure may produce different TFCOH resolution and sensitivity. In general, an arbitrary spectral decomposition approach (the Fourier or wavelet transform) can be used to estimate cross spectra and power spectrum. In the literature, wavelet coherence is most considered[7,16,28,11,23,19,32]. Note that, conventional method indicates that $S^{\star}(.)$ **and** $S^{\star\star}(.)$ **both are equal, and hence numerator and denominator of Eq.**(4) **are identically smoothed**. The generalization of the coherencye function presently proposed is obtained by relaxing the constraint that $S^{\star}(.) = S^{\star\star}(.)$. By letting $S^{\star}(.) \neq S^{\star\star}(.)$, we

introduce two possible solutions for the estimation of TFCOH. These two solutions are presented by Methods 2 and 3, respectively.

2.3.2. ***Method 2***

The first solution is achieved when the rectangular window $h^{\star}[l^{\star}]$ becomes very narrow, for instance $l^{\star} = 1$, and $h^{\star\star}[l^{\star\star}]$ becomes very wide, i.e., $l^{\star\star} \geq 2T - 1$. That is, the size of the integration window $h^{\star\star}[l^{\star\star}]$ is greater than the time duration of $s_x[n, f]$. Hence, from convolution theorem perspective and by restricting the convolved signal to the **same** time duration of $s_x[n, f]$, Eq.(5) becomes Eq.(7).

$$\begin{aligned} S^{\star}(s_{xy}[n, f]) &= s_{xy}[n, f] \circledast 1 = s_{xy}[n, f] \\ S^{\star\star}(s_x[n, f]) &= \sum_{m=1}^{T} s_x[m, f] \end{aligned} \tag{7}$$

By dividing the sum in Eq.(7) by T, the averaged power spectrum is achieved at specific frequency f. That is, TFCOH is estimated by normalizing the non-smoothed cross spectra by the product of ensemble averaged power spectra. This product is first estimated using Welch's method[31], implying that TFCOH is estimated by normalizing a complex cross spectra estimated at segment n by;

$$\hat{\Gamma}_{xy}[n, f] = T \frac{s_{xy}[n, f]}{\sqrt{\sum_{m=1}^{T} s_x[m, f] \sum_{m=1}^{T} s_y[m, f]}}, \; n = 1, 2, .., T \tag{8}$$

By averaging $\hat{\Gamma}_{xy}[n, f]$ over n, we obtain the coherency expressed by Eq.(1). Thus, Eq.(8) gives the time-resolved estimate of coherency. We note that, the temporal average of Method 1 does not equate with standard coherency.

2.3.3. ***Method 3***

The second solution is closely related to the Method 2. The aim of Method 3 is to improve the statistical consistency (e.g., robustness of TFCOH estimators against noise) of Eq.(8) by smoothing the cross spectra. For this, a smoothed TFCOH is estimated by substituting numerator of Eq.(4) into the numerator of Eq.(8) :

$$\hat{\Gamma}_{xy}[n,f] = T\frac{S^{\star}\left(s_{xy}[n,f]\right)}{\sqrt{\sum_{m=1}^{T} s_x[m,f]\sum_{m=1}^{T} s_y[m,f]}} \tag{9}$$

If TFCOH expressed in Methods 2 and 3 are estimated in the presence of independent identically distributed (*i.i.d*) noise (e.g., white noise sequence with mean zero and unit variance), then two distinct time and frequency based covariance matrices are estimated at time lag, 0, to eliminate the influence of noise in the TFCOH plane. Hence, we have:

$$\hat{\Gamma}_{xy}[n,f] = \hat{\gamma}_{xy}[n,f] + \eta[n,f] \tag{10}$$

where $\hat{\gamma}_{xy}[t,f]$ denotes the noise-free TFCOH, and $\eta[n,f]$ is the noise coherency, such that $\mathbb{E}\{\eta[n,f]\} = 0, \forall f,n$, where $\mathbb{E}$ is the expectation operator. Then, the *time-based covariance matrix* of $\hat{\Gamma}_{xy}[n,f]$ is estimated as $\hat{R}_{xy}[n,n] = \mathbb{E}\{\hat{\Gamma}_{xy}[n,f]\hat{\Gamma}^{T_r}_{xy}[n,f]\}$, where T_r refers to matrix transposition. Similarly, the *frequency-based covariance matrix* is estimated by $\hat{R}_{xy}[f,f] = \mathbb{E}\{\hat{\Gamma}^{T_r}_{xy}[n,f]\hat{\Gamma}_{xy}[n,f]\}$. In consequence, the time-based covariance

matrix that gives an estimation of noise-free time-course of the coherency, is obtained by

$$\begin{aligned}\mathbb{E}\{\hat{\Gamma}_{xy}[n,f]\hat{\Gamma}_{xy}^{T_r}[n,f]\} &\equiv \mathbb{E}\Big\{\big(\hat{\gamma}_{xy}[n,f]+\eta[n,f]\big)\\ &\quad \big(\hat{\gamma}_{xy}[n,f]+\eta[n,f]\big)^{T_r}]\Big\}\\ &\equiv \mathbb{E}\Big\{\hat{\gamma}_{xy}[n,f]\hat{\gamma}_{xy}^{T_r}[n,f]\Big\}\\ &+\big(\,\mathbb{E}\{\eta_{xy}[n,f]\}\,\mathbb{E}\{\eta_{xy}^{T_r}[n,f]\}\big)\\ &\equiv \mathbb{E}\{\hat{\gamma}_{xy}[n,f]\hat{\gamma}_{xy}^{T_r}[n,f]\}\end{aligned} \tag{11}$$

Note that, noise components are deflated due to their independency.

2.3.4. ***Wavelet coherency***

Alternatively, wavelet functions can also be used for spectral decomposition rather than Fourier-based methods used in Eqs.(4) , (8), and (9). Hence, the equivalent of Methods 1, 2, and 3 can be defined for wavelet coefficients. We shortly describe these variations below and demonstrate its use in the experimental data. Following[23,32], and similar to Eq.(4), the bivariate continuous wavelet coherency of two continuous-time signals $x(t)$ and $y(t)$ at location b and scale a is estimated as follows:

$$\hat{\Gamma}_{xy}(b,a) = \frac{S^{\star}\Big(w_{xy}(b,a)\Big)}{\sqrt{S^{\star\star}\Big(\,|w_x(b,a)|^2\,\Big)S^{\star\star}\Big(\,|w_y(b,a)|^2\,\Big)}} \tag{12}$$

where $S^{\star}\Big(w_{xy}(b,a)\Big)$ denotes the smoothed wavelet cross-spectra, and $S^{\star\star}\Big(\,|w_x(b,a)|^2\,\Big)$ and $S^{\star\star}\Big(\,|w_y(b,a)|^2\,\Big)$ are both smoothed wavelet power spectra. The wavelet power spectrum is usually computed by square of the magnitude of wavelet transform (see Eq.(13)). The WT of discrete-time signal, $x[p]$, $p = 0, 1, 2, ..., L-1$, is computed by convolving $x[p]$ with a scaled and translated version of a mother wavelet

function $\psi_{a,b}[p]$:[28]

$$w_x(a,b) = \frac{1}{\sqrt{|a|}} \sum_{p=0}^{L-1} x[p]\psi^* \left(\frac{p-b}{a} \right) \tag{13}$$

The result of convolution in Eq.(13) is the inverse Fourier transform of the product of the DFT of discrete-time signal $x[p]$ with DFT of a mother wavelet, for instance, the complex Morlet wavelet, $\psi(t) = \pi^{-1/4} e^{j2\pi\omega_0(t)} e^{-t^2/2}$. Therefore, Eq.(13) can be written as[28]:

$$w_x(a,b) = \sqrt{|a|} \sum_{f=0}^{N-1} F_x(f) F_{\psi^*}(a\kappa) e^{j2\pi fb} \tag{14}$$

Where $F_x(f)$ denotes the DTF of $x[p]$, and $F_{\psi^*}(af)$ is the DFT of the complex conjugate of $\psi(af)$ at scale a. The relationship between the equivalent Fourier period (or Fourier frequency) and the Morlet wavelet scale is given by $f = 4\pi a / \left(\omega_0 + \sqrt{2+\omega_0^2} \right)$[28]. As a consequence of the above description, we write $f \propto (a)$ and $t \propto (b,n)$. These proportions provide appropriate replacements for the scale and translation parameters with their analogues frequency and time, respectively. Therefore, the discrete version of wavelet TFCOH analogue with Eqs.(8) and (9) are respectively given by:

$$\hat{\Gamma}_{xy}[n,f] = \frac{w_{xy}[n,f]}{\sqrt{\left\langle \left| w_x[n,f] \right|^2 \right\rangle \left\langle \left| w_y[n,f] \right|^2 \right\rangle}} \tag{15}$$

$$\hat{\Gamma}_{xy}[n,f] = \frac{S^\star \Big(w_{xy}[n,f] \Big)}{\sqrt{\left\langle \left| w_x[n,f] \right|^2 \right\rangle \left\langle \left| w_y[n,f] \right|^2 \right\rangle}} \tag{16}$$

where $\langle . \rangle$ denotes the average operator. Note that, cross wavelet spectra are normalized by the product of the averaged wavelet power spectra at each specific frequency f.

2.4. ***Simulated and Experimental Data***

Two simulated signal pairs with different properties were generated to study the three different TFCOH representations:

1. A signal pair with time-varying coherence, e.g., modulated Gaussian noise at frequency 0.6Hz

2. A signal pair with frequency-varying coherence, e.g., a jump in synchronous frequencies from 10Hz to 20Hz, over time.

We also sought to explore the different ability of these three methods to characterize dynamic coherence in an examplar complex physiological signal, namely human EEG data.

2.4.1. ***Simulated Data, Example 1 (Time-varying coherence)***

Two independent noise sequences $\{\alpha_{1_m}\}_{m=1}^{M}$ and $\{\alpha_{2_m}\}_{m=1}^{M}$ with mean 0 and variance 1 were modulated by a sinusoid signal $\beta[m]$, where M is the total number of samples. This modulation produces two signals $S_3[m] = \alpha_1[m] + \beta[m]\alpha_2[m]$, and $S_4[m] = \alpha_2[m] + \beta[m]\alpha_1[m]$, which are synchronized and desynchronized over time[19]. We defined a pure sinusoid signal $\beta[m]$ as $\beta[m] = a(1 + \sin[2\pi 0.6m])$. The amplitude a determines the boundaries of the coherence, (see Eq.(17)). Since $\alpha_1[m]$ and $\alpha_2[m]$ are Gaussian noise with variance $\sigma^2 = 1$, the power-spectra of α_1 and α_2 are both equal to $\sigma^2 = 1$ for all frequencies, and their cross-spectra is equal to 0. The coherence between signals $S_3[m]$ and $S_4[m]$ can be analytically defined as a function of $\beta[m]$ as:

$$\Gamma[a, m] = \frac{4a^2F^2[m]}{(1 + a^2F^2[m])^2} \tag{17}$$

where $F[m] = \frac{1}{a}\beta[m]$, and $a \in [0.01, 0.5]$. By substituting $a_{max} = 0.5$ and $a_{min} = 0.01$ into Eq.(17), one respectively obtained two bounds for time-varying coherence, one is $0 \leq \Gamma[0.5, m] \leq 1$, and the other $0 \leq \Gamma[0.01, m] \leq 1.6 \times 10^{-3}$.

Methods 1, 2, and 3 were employed to estimate time-varying coherence under the amplitude condition $a \in [0.01, 0.5]$. To assess the performance of methods, statistical measures

including sensitivity, specificity, and z-score are also calculated with confidence interval (CI= 50%). We used CI= 50% to binarize the coherency spectra for the purpose of computing the sensitivity and specificity.

2.4.2. ***Simulated Data, Example 2 (Frequency-varying coherence)***

We simulated two independent signals $S_1[m] = \Big[x_1[m_1]+\eta_1[m_1], x_2[m_2]+\eta_2[m_2]\Big]$ and $S_2[m] = \Big[x_1[m_2]+\eta_3[m_2], x_2[m_1]+\eta_4[m_1]\Big]$ of length 20sec. Note that $m_1 = 12$sec, and $m_2 = 8$sec. $\eta[m]$ is Gaussian noise: $\eta[m] \sim \mathbf{N}(\mu_\eta = 0, \sigma_\eta^2 = 1)$. Two sinusoid signals $x_1[m] = A\sin[2\pi 10m]$ and $x_2[m] = A\sin[2\pi 20m]$ were contaminated by four independent Gaussian noise $\eta_i[m], i = 1, 2, 3, 4$ as stated above. To produce signals with different amplitudes, we defined a range of amplitudes A by using a wide range of Signal-to-Noise Ratio (SNR) as:

$$A = A_{noise}\left(10^{\frac{SNR}{20}}\right) \tag{18}$$

where $SNR \in [-30, 10]$dB, where dB is a logarithmic unit that indicates the ratio of a physical quantity (noise strength, signal strength, etc). Noise amplitude is $A_{noise} \in \mathbb{R}$. In this paper, we set $A_{noise} = 0.2\sqrt{2}\ mV$. To assess performance of Methods 1, 2, and 3 in the measurement of TFCOH in the presence of a wide range of noise strengths, statistical measures including sensitivity and specificity were calculated. Sensitivity is defined by $Sensitivity = \frac{TP}{TP+FN}\%$ (as a measure of the method's ability to detect true TFCOH), and specificity is expressed by $Specificity = \frac{TN}{TN+FP}\%$ (as a measure of the method's ability to successively exclude non-coherence). TP, TN, FP and FN denote number of true positives, true negatives, false positives, and false negatives, respectively. Furthermore, a quantitative assessment of the robustness of Methods 1, 2, and 3 against white noise, was carried out by z-scores at each specific noise strength. To determine

the values of significant threshold, sensitivity, and specificity for TFCOH at CI= 50%, surrogate data were used. We employed the technique of linear surrogate data generation given in[4], namely derived through the Fourier phases of signals $S_1[m]$ and $S_2[m]$. TFCOH of surrogate data was generated for 100 repetitions at each specific noise strength.

2.4.3. ***Experimental Data (Human EEG)***

We also sought an exploratory assessment of the TFCOH estimators (Methods 1, 2, and 3) in characterizing synchronization in an exemplar physiological dataset, namely human EEG. To be precise, we studied TFCOH between the two scalp channels over occipital cortex (O_1 and O_2). Subjects were requested to sit still with eyes close for 10 minutes. EEG data was acquired from three healthy human subjects at sampling frequency $Fs = 500$Hz and digitized by an analog to digital convertor (ADC) with resolution of 16 $bits/sample$. The protocol was approved by the Human Research Ethics Committee of The University of New South Wales. All subjects gave voluntary and informed consent according to National Health and Medical Research Council guidelines. Acquired EEG signals were passed through a band pass filter with cut-off frequencies $[0.01, 250]$Hz prior to analysis. This data were chosen because it is known to contain complex patterns of intermittent synchronization within and between channels within the alpha frequency range (8-13 Hz). Full details of data acquisition and preprocessing can be found in[12].

3. Results

We first report the validation and comparison of the Methods in simulated data, whose time frequency properties are known through construction. We then report an exploratory analysis of the TFCOH methods in human EEG.

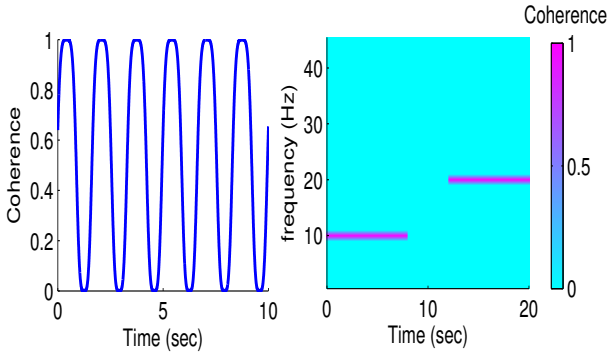

Figure 1: Left panel represents the analytic time-varying coherence obtained from Eq.(17) at amplitude $a = 0.5$, and the desired TFCOH (right panel) for the frequency-varying coherence described in Example 2.

3.1. ***Simulation results***

Fig.1 shows the analytic time-varying coherence obtained from Eq.(17) at amplitude $a = 0.5$ for Example 1, and the desired TFCOH (right panel) for the frequency-varying coherence described in Example 2. TFCOH estimates based on Method 1, 2, and 3 for the simulated data described in Example 1 are depicted in Fig.2. Overall, Methods 2 and 3 could detect the lower bound of the coherence near 0.15, whereas Method 1 failed to measure TFCOH< 0.4 as shown in the right panels. That is, Methods 2 and 3 facilitated the detection of a wider range of coherence compared to Method 1. Similarly, percentage of TFCOH obtained from Methods 2 and 3 indicate coverage of a wider range of the coherence boundaries. In Fig.3 sensitivity (top row), specificity (middle row), and z-score (lower row) of all three methods are represented at $f_1 = 0.6$Hz (left column) and $f_2 = 1.2$Hz (right column), respectively. In general, Method 1 has the highest sensitivity at both frequencies due to high TP rate and a low number of TN compared to Methods 2 and 3. In other words, the effects of the variance and bias of Method 1 are reflected in the lower false negative rate (higher sensitivity) which comes at the cost of higher rate

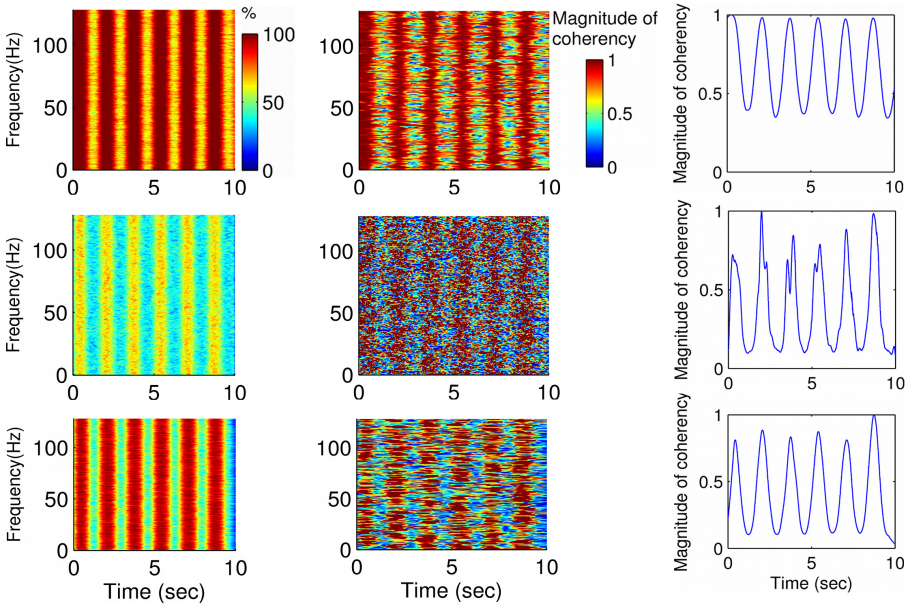

Figure 2: Time-varying synchronization of simulated data described in Example 1 using Methods 1, 2, and 3 (top to bottom row, respectively). Left column represents the percentage of significant time-frequency points at 50% confidence interval estimated across 100 simulations. Middle column shows raw TFCOH estimates of a single trial. Right column represents time-course of the coherence (i.e., magnitude of coherency as function of the time) at specific amplitude $a = 0.5$ defined in Eq.(17) obtained from the main diagonal of the time-based covariance matrix.

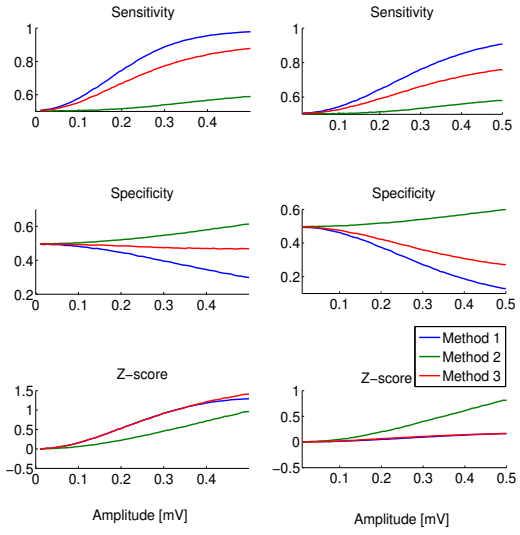

Figure 3: The sensitivity (top row), specificity (middle row), and z-scores (lower row) of the Methods 1, 2, and 3, at frequencies $f_1 = 0.6$Hz (left column) and $f_2 = 1.2$Hz (right column), respectively.

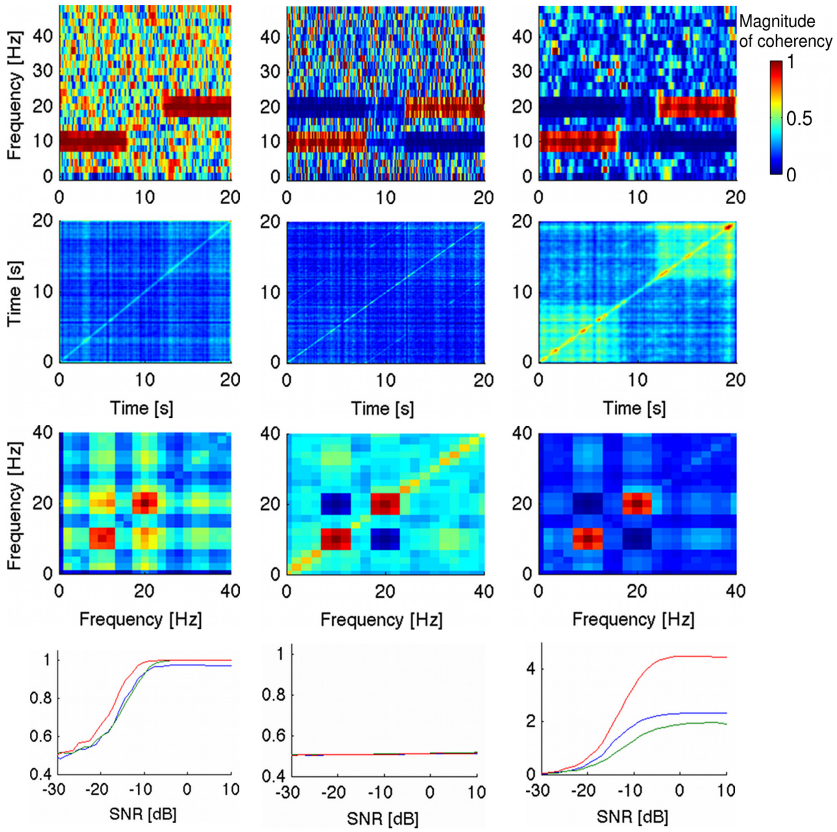

Figure 4: Results from Methods 1, 2, and 3 (left to right column, respectively) of simulated data described in Example 2. Top row (left to right panels) represents TFCOH for a single trial at $SNR = 0$dB based on Methods 1, 2, and 3, respectively. Two middle rows show the time and frequency based covariance matrices using Eq.(11) at $SNR = 0$dB. The bottom row represents the sensitivity, specificity, and z−scores in the interval of $SNR \in [-30,\ 10]dB$ for all three methods across 100 simulations.

of false positives (lower specificity) than Methods 2 and 3 in the case of time-varying coherence. This is further underscored by the lower specificity of Method 1. Robustness and stability of Method 3 against white noise modulated by carrier frequency $f_1 = 0.6$Hz is better than the other 2 methods as reflected by the higher z-score value. This was changed for carrier frequency $f_2 = 1.2$Hz. That is, Method 2 reveals the highest stability and robustness against noise, reflecting its superior temporal resolution due to the non-smoothed cross spectra. Fig.4 represents TFCOH estimates obtained using Methods 1, 2, and 3 for the simulated data described in Example 2. Although all methods show the synchronous frequencies at $f_1 = 10$Hz (from $t = 0$ to $t = 8$sec) and $f_2 = 20$Hz (from

$t = 12$ to $t = 20$sec), the results obtained by Methods 2 and 3 appeared more robust at $SNR = 0$dB compared to Method 1. The next two rows represent time-based and frequency-based covariance matrices using Eq.(11). Method 3 has improved statistical consistency in revealing the time-course of the coherence represented by the time-based covariance matrix. In addition, frequency-based covariance matrices implied Methods 2 and 3 to be consistent in detecting synchronous frequencies by avoiding the construction of spurious synchronous frequencies. Spurious synchronous frequencies appeared in the off-diagonals of the frequency-based covariance matrix of Method 1 at $f_1 = 10$Hz and $f_2 = 20$Hz. In contrast, Methods 2 and 3 only represented the synchronous frequencies (10 and 20Hz) along their main diagonals. Bottom row shows the result of sensitivity, specificity, and z-score measurements. Method 3 yields better sensitivity compared to Method 1. In addition, Method 2 rendered higher sensitivity at interval of $SNR \in [-10, 10]$dB compared to Method 1. For example, sensitivity of methods 2 and 3 at $SNR = -5$dB are 1, whereas Method 1 showed sensitivity ≈ 0.95. This gap is remained consistent until $SNR = 10$dB. Specificity of all methods approximately agreed. Method 3 had the highest z-score, approximately $z_{score} = 4.2$ at $SNR = -3$dB indicating its robustness and stability against noise strength. Combining these results signifies that presently proposed technique (i.e., Methods 2 and 3) has an improved trade-off between statistical consistency and temporal resolution of TFCOH. This enables better recognition of (linear) correlations in the presence of noise. Comparing the analytic solution for the time-varying coherence (Fig.1, left panel) and the estimated one (Fig.2, right column) indicates that Methods 2 and 3 estimated a broader range of the coherence, in particular, the lower coherence rate where Method 1 fails. Similarly, TFCOH of Example 2 estimated

by Methods 2 and 3 (Fig.4, top row, the last two right panels) show lower bound of the coherency where Method 1 shows noisy TFCOH.

3.2. ***Experimental results***

As mentioned earlier, we sought to compare the TFCOH estimators (e.g., Methods 1, 2, and 3) in characterizing dynamic patterns of coherence between regions of human occipital cortex, as reflected in surface electrode recordings at O_1 and O_2 channels. For the EEG analyses, we only used the imaginary part of TFCOH to avoid the spurious synchronization due to volume conduction. Previous studies have shown that the imaginary part reflects genuine neural interactions in electrophysiological recordings and it is unaffected by volume conduction[20,26]. The results are shown in Fig.5. An example of the EEG recordings is provided in the top row. Results for Methods 1,2 and 3 are shown below in the left, middle and right column respectively. The second row shows the Fourier-based TFCOH plots for each method whereas the third row represents the corresponding wavelet-based results (notice the adaptive tessellation of the time-frequency plane). When visually comparing the methods, it is clear that Method 1 (both Fourier and wavelet-based variants) shows uniformly higher coherency at all frequencies and times: There appears to be reduced information. The most specific results appear to be in the wavelet-based TFCOH plane derived from method 3, where discrete instances of high coherency intermittently appear within the alpha ($8-13$Hz) frequency range. The two bottom rows show the frequency-based covariance matrices of each of the three methods derived from the entire time series. Method 1 - both wavelet and Fourier-based - indicate coherence across a broad range of frequencies (e.g., $f < 10$Hz). In contrast, Methods 2 and 3 both indicate that there is a specific coherent frequency between the two EEG sig-

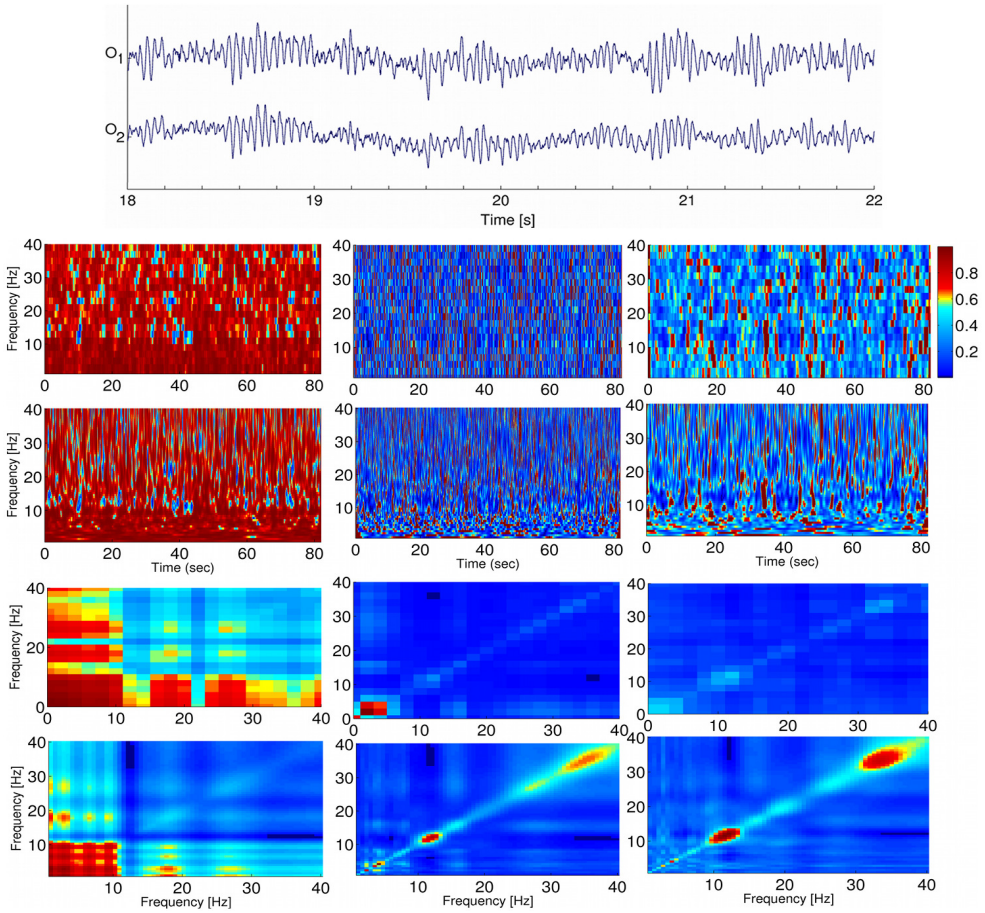

Figure 5: Fourier and wavelet TFCOH between two occipital EEG channels, O_1 and O_2 measured by Methods 1 (left column), 2 (middle column), and 3 (right column). Top row shows an example of the bivariate time series. Next two rows show the imaginary part of the Fourier- and wavelet-based TFCOH results. The two lower rows show the frequency-based covariance matrices for the Fourier (top) and wavelet (bottom) TFCOHs. Note the striking coherence at both 10 and 35 Hz evident most clearly when using Method 3 in conjunction with the wavelet transform (very lower right panel).

nals, O_1 and O_2 isolated to the alpha frequency range. Furthermore, the frequency-based covariance matrix of wavelet TFCOH, using Method 3 in particular, suggests coherence about approximately 35Hz, in the so-called gamma frequency range (see Fig.5, bottom row). Gamma-band synchronization in visual cortex has previously been observed using invasive recording techniques and extensively discussed in literature[15,13]. The detection of gamma-band synchronization in single-trial EEG data obtained from surface recordings underscores the robustness and sensitivity of the proposed method. The TFCOH of the other two subjects showed similar effects, i.e. coherency at both alpha and higher frequencies, evident most strikingly when using Method 3.

4. Conclusion

In the present paper, we proposed a generalized time-frequency coherency function to improve the estimation of TFCOH in single-trial data. Generalization of the coherency function was obtained by relaxing the constraint of using identical smoothing operators for the cross and auto spectra. This opens broader possibilities in the estimation of TFCOH. This novel approach improves the trade-off between time-frequency resolution and statistical consistency by reducing the negative side effect of smoothing of the power spectrum. Specifically, TFCOH is estimated by normalizing the non-smooth temporal cross-spectra by the product of ensemble averaged power spectra. We showed that the method gives the time-resolved estimation of the classic coherence function. Efficiency was tested in two simulated data sets involving time-varying and frequency-varying correlations using statistical tests, i.e. sensitivity, specificity and z-score. Our method rendered the highest statistical consistency against a wide range of noise strength compared to the conventional approach. In experimental study, TFCOH was estimated between two oc-

cipital EEG signals, which revealed that our method could exclusively extract alpha- and gamma-band synchronization in visual cortex from single-trial data. As such, the proposed method appears particularly suitable for assessing functional connectivity in resting-state EEG.

5. Acknowledgments

This study was funded by the Thinking Systems Initiative (ARC TS0669860) and the Netherlands Organisation for Scientific Research (NWO 451-10-030).

6. References

[1] Aydin, S.. Comparison of power spectrum predictors in computing coherence functions for intracortical EEG signals. Annals of Biomedical Engineering 2009;37(1):192–200.

[2] Bigot, J., Longcamp, M., Dal Maso, F., Amarantini, D.. A new statistical test based on the wavelet cross-spectrum to detect time-frequency dependence between non-stationary signals: Application to the analysis of cortico-muscular interactions. NeuroImage 2011;55(4):1504–1518.

[3] Boonstra, T., Daffertshofer, A., Breakspear, M., Beek, P.. Multivariate time-frequency analysis of electromagnetic brain activity during bimanual motor learning. NeuroImage 2007;36(2):370–377.

[4] Breakspear, M., Brammer, M., Robinson, P.A.. Construction of multivariate surrogate sets from nonlinear data using the wavelet transform. Physica D: Nonlinear Phenomena 2003;182(1-2):1–22.

[5] Breakspear, M., Stam, C.J.. Dynamics of a neural system with a multiscale architecture. Phil Trans R Soc B 2005;36:1051–1074.

[6] Brillinger, D.R.. Time Seris Data Analysis and Theory. Number 36, pp.297-300. University Science Center, Philadelphia, PA, 19104-2688: SIAM's Classics in Applied Mathematics, 2001.

[7] Brittain, J.S., Halliday, D., Conway, B., Nielsen, J.. Single-trial multiwavelet coherence in application to neurophysiological time series. IEEE Transactions on Biomedical Engineering 2007;54(5):854–862.

[8] Bruns, A.. Fourier-, Hilbert- and wavelet-based signal analysis: are they really different approaches? Journal of Neuroscience Methods 2004;137.

[9] Buzsaki, G., Draguhn, A.. Neuronal oscillations in cortical networks. Science 2004;304(5679):1926–1929.

[10] Carter, G.. Coherence and time delay estimation. Proceedings of the IEEE 1987;75(2):236–255.

[11] Cohen, E., Walden, A.. A statistical study of temporally smoothed wavelet coherence. IEEE Transactions on Signal Processing 2010;58(6):2964–2973.

[12] Freyer, F., Aquino, K., Robinson, P.A., Ritter, P., Breakspear, M.. Bistability and non-gaussian fluctuations in spontaneous cortical activity. Journal of Neuroscience 2009;29(26):8512–8524.

[13] Fries, P., Reynolds, J., Rorie, A., Desimone, R.. Modulation of oscillatory

neuronal synchronization by selective visual attention. Science 2001;291(5508):1560–1563. Cited By (since 1996) 749.

[14] Gabor, D.. Theory of communication. J IEE London 1946;93:429–457.

[15] Gray, C., Konig, P., Engel, A., Singer, W.. Oscillatory responses in cat visual cortex exhibit inter-columnar synchronization which reflects global stimulus properties. Nature 1989;338(6213):334–337. Cited By (since 1996) 1538.

[16] Grinsted, A., Moore, J., Jevrejeva, S.. Application of the cross wavelet transform and wavelet coherence to geophysical times series. Nonlinear Processes in Geophysics 2004;11(5-6):561–566.

[17] Hlawatsch, F., Boudreaux-Bartels, G.. Linear and quadratic time-frequency signal representations. IEEE Signal Processing Magazine 1992;9(2):21–67.

[18] Jiang, X., Mahadevan, S.. Wavelet spectrum analysis approach to model validation of dynamic systems. Mechanical Systems and Signal Processing 2011;25(2):575–590.

[19] Lachaux, J.P., Lutz, A., Rudrauf, D., Cosmelli, D., Le Van Quyen, M., Martinerie, J., Varela, F.. Estimating the time-course of coherence between single-trial brain signals: An introduction to wavelet coherence. Neurophysiologie Clinique 2002;32(3):157–174.

[20] Nolte, G., Bai, O., Wheaton, L., Mari, Z., Vorbach, S., Hallett, M.. Identifying true brain interaction from EEG data using the imaginary part of coherency. Clinical Neurophysiology 2004;115(10):2292–2307.

[21] Rosenberg, J., Amjad, A., Breeze, P., Brillinger, D., Halliday, D.. The Fourier approach to the identification of functional coupling between neuronal spike trains. Progress in Biophysics and Molecular Biology 1989;53(1):1–31.

[22] Salant, Y., Gath, I., Henriksen, O.. Prediction of epileptic seizures from two-channel EEG. Medical and Biological Engineering and Computing 1998;36(5):549–556.

[23] Santoso, S., Powers, E., Bengtson, R., Ouroua, A.. Time-series analysis of nonstationary plasma fluctuations using wavelet transforms. Review of Scientific Instruments 1997;68(1):898–901.

[24] Schnitzler, A., Gross, J.. Normal and pathological oscillatory communication in the brain. Nature Reviews Neuroscience 2005;6(4):285–296.

[25] Schoffelen, J.M., Oostenveld, R., Fries, P.. Neuronal coherence as a mechanism of effective corticospinal interaction. Science 2005;308(5718):111–113.

[26] Stam, C., Nolte, G., Daffertshofer, A.. Phase lag index: Assessment of functional connectivity from multi channel EEG and MEG with diminished bias from common sources. Human Brain Mapping 2007;28(11):1178–1193.

[27] Stoica, P., Moses., R.. Spectral Analysis of Signals. pp.67-68. Upper Saddle River, New Jersey, 07458: Pearson Prentice Hall, 2005.

[28] Torrence, C., Compo, G.. A practical guide to wavelet analysis. Bulletin of the American Meteorological Society 1998;79(1):61–78.

[29] Torrence, C., Webster, P.. Interdecadal changes in the enso-monsoon system. Journal of Climate 1999;12(8 PART 2):2679–2690.

[30] Varela, F., Lachaux, J.P., Rodriguez, E., Martinerie, J.. The brainweb: Phase synchronization and large-scale integration. Nature Reviews Neuroscience 2001;2(4):229–239.

[31] Welch, P.D.. The use of Fast Fourier Transform for the estimation of power spectra: A method based on time averaging over short, modified periodograms. IEEE Transaction on Audio Electroacoust 1967;AU-15:70–73.

[32] Yang, Q., Siemionow, V., Yao, W., Sahgal, V., Yue, G.. Single-trial EEG-EMG coherence analysis reveals muscle fatigue-related progressive alterations in corticomuscular coupling. IEEE Transactions on Neural Systems and Rehabilitation Engineering 2010;18(2):97–106.